Chapter 2

Astronomical pacing of late Paleocene to early Eocene global warming events

At the boundary between the Paleocene and Eocene epochs, about 55 million years ago, the Earth experienced a strong global warming event, the Paleocene–Eocene thermal maximum (Kennett and Stott, 1991; Koch et al., 1992; Norris and Röhl, 1999; Zachos et al., 2001). The leading hypothesis to explain the extreme greenhouse conditions prevalent during this period is the dissociation of 1,400 to 2,800 gigatonnes of methane from ocean clathrates (Dickens et al., 1997), resulting in a large negative carbon isotope excursion and severe carbonate dissolution in marine sediments. Possible triggering mechanisms for this event include crossing a threshold temperature as the Earth warmed gradually (Thomas and Schackleton, 1996; Dickens et al., 1995), comet impact (Kent et al., 2003), explosive volcanism (Bralower et al., 1997; Schmitz et al., 2004) or ocean current reorganization and erosion at continental slopes (Katz et al., 2001), whereas orbital forcing has been excluded (Cramer et al., 2003). Here we report a distinct carbonate-poor red clay layer in deep-sea cores from Walvis ridge (Zachos et al., 2004), which we term the *Elmo* horizon. Using orbital tuning, we estimate deposition of the *Elmo* horizon at about 2 million years after the Paleocene–Eocene thermal maximum. The *Elmo* horizon has similar geochemical and biotic characteristics as the Paleocene–Eocene thermal maximum, but of smaller magnitude. It is coincident with carbon isotope depletion events in other ocean basins, suggesting that it represents a second global thermal maximum. We show that both events correspond to maxima in the ~405-kyr and ~100-kyr eccentricity cycles that post-date prolonged minima in the 2.25-Myr eccentricity cycle, implying that they are indeed astronomically paced.

Biotic phenomena similar to those characterizing the Paleocene–Eocene thermal maximum (PETM) have been locally recorded in the upper Paleocene to lower Eocene, indicating the possibility of additional hyperthermal events, though of smaller magnitude (Bujak and Brinkhuis, 1998; Thomas and Zachos, 2000; Röhl et al., 2003). Several short, negative carbon isotope shifts of up to 1‰ at deep-sea sites resemble the much larger-amplitude carbon isotope excursion at the PETM (Cramer et al., 2003). Orbital tuning suggested that these transients were controlled by maxima in the short-term eccentricity cycles, whereas the PETM carbon isotope excursion allegedly occurred near a minimum in the ~405-kyr eccentricity cycle, excluding orbital forcing as a triggering mechanism for the latter (Cramer et al., 2003).

One objective of Ocean Drilling Program (ODP) Leg 208 on the Walvis ridge (subtropical southeastern Atlantic Ocean) was to search for hyperthermal events within the lower Cenozoic greenhouse climate record. We recovered continuous, undisturbed lower Paleogene successions at five sites along a 2-km water depth transect in multiple (mostly advanced piston core) holes (Zachos et al., 2004). This resulted in the first complete early Paleogene deep-sea record accumulated at relatively high sedimentation rates. The uppermost Paleocene and lower Eocene are composed of foraminifer-bearing nannofossil ooze, with a few chert layers and two deep-red clay layers marking the PETM and a younger distinctive horizon, named *Elmo*. Magnetobiostratigraphic results on Site 1262 (see Appendix 2) reveal that the *Elmo* horizon at 117.1–117.2 m composite depth (m.c.d.) is slightly older than the chron C24r/C24n reversal boundary (115–116 m.c.d.) (Appendix Fig. 2.1) and occurs within the lower part of NP11.

The *Elmo* horizon is 10–15 cm thick, and characterized by elevated magnetic susceptibility (MS) values at all sites (Fig. 1). Analysis of the $CaCO_3$ content (expressed in weight per cent: wt%) of the deepest Site 1262 (paleodepth, 3,600 m), intermediate Site 1266 (paleodepth, 2,600 m) and shallowest Site 1263 (paleodepth, 1,500 m) reveal that the increase in MS is linearly related to a drop in $CaCO_3$ wt% (Appendix Fig. 2.2). The $CaCO_3$ wt% declines from 90–95 below, to ~40% within, the red clay. High-resolution bulk carbon isotope records ($\delta^{13}C_{bulk}$) of Sites 1262, 1265, 1266 and 1267 reveal a negative excursion of 1.0–1.2‰ from below the first decline in $CaCO_3$ wt% into the *Elmo* (Fig. 1). The $\delta^{13}C_{bulk}$ of Site 1263 shows the largest depletion (1.4–1.6‰), suggesting that the red clay layer at this site with the highest sedimentation rate (Zachos et al., 2004) is stratigraphically the most complete and/or least affected by the dissolution of primary calcite and the presence of reworked or secondary calcite. The post-*Elmo* interval mirrors the typical PETM signature with an exponential recovery to pre-excursion $\delta^{13}C_{bulk}$ values. The bulk carbonate oxygen isotope record ($\delta^{18}O_{bulk}$) of Site 1263 shows a negative excursion of ~1.6‰ (Fig. 2).

From Site 1263, we analysed the stable isotopic composition of individual specimens (>300 μm size fraction) of the surface-dwelling planktonic foraminifer *Acarinina soldadoensis* and the benthic foraminifers *Cibicidoides* spp. and *Anomalinoides* spp. (Fig. 2). The planktonic foraminiferal data show a much larger inter-specimen variability within each sample (especially within the *Elmo* horizon) than the benthic data. The (smoothed) carbon isotope record of *A. soldadoensis* ($\delta^{13}C_{A.soldadoensis}$) resembles the pattern of the bulk record, but shows a significantly larger negative excursion (~2.5‰). The carbon isotope shift is much smaller in the benthic foraminiferal record than in *A. soldadoensis*, but the (~1‰) trend through the carbonate-rich intervals equals that of the bulk and planktonic isotope records. Benthic foraminifera species richness is low and assemblages are dominated by diminutive *Nuttallides truempyi* and *Abyssamina* spp. species in the *Elmo* horizon. The few measured benthic isotope values of the *Elmo* horizon, representing *Anomalinoides* spp. specimens (*Cibicidoides* spp. >300 μm are absent in the *Elmo* horizon), are similar to those from outside the clay layer, indicating that these are likely derived from bioturbated specimens. This suggests that large-sized benthic foraminifera were absent during deposition of the *Elmo* horizon, as commonly observed for the PETM (Thomas et al., 2000). The presence of light-coloured burrows within the red clay layer documents bioturbation, and could explain the scatter in the planktonic isotope values, and the less strong $\delta^{13}C_{bulk}$ excursion relative to $\delta^{13}C_{A.soldadoensis}$. This possibility does not rule out that the magnitude of the excursion in the deep sea could have been damped owing to the larger carbon mass of this reservoir. The maximum oxygen isotope shift in *A. soldadoensis* ($\delta^{18}O_{A.soldadoensis}$) across the *Elmo* horizon is comparable to that of the $\delta^{18}O_{bulk}$ record. There is only a ~0.6‰ shift in the benthic oxygen isotope record, either because no *in situ* large benthic foraminifera are present in the *Elmo* horizon or changes in bottom water temperatures were minor.

To unravel the orbital relationship between the *Elmo* horizon and PETM, we studied the cyclic sedimentary patterns of the interlaying interval in continuous spliced cores derived from advanced piston core holes only. Spectral analysis was applied on the colour reflectance (*L**) of Site 1267, and *L** and MS of Site 1262 (see Appendix 2). The spectra of all records revealed the dominance of the long (~405-kyr) and short (~100-kyr) eccentricity cycles (Appendix Fig. 2.3) Both components were extracted and could be unambiguously correlated between the records of these sites (Fig. 3). Four long-term maxima in MS (minima in *L**) occur between the *Elmo* horizon and PETM. The *Elmo* horizon corresponds to a fifth long-term MS maximum (*L** minimum) and a short-term MS maximum (*L** minimum) cycle. The red clay layer associated with the PETM ends in a long-term MS minimum (*L** maximum). If there were 11 climate precession cycles in the PETM interval (Röhl et al., 2000), then its carbon isotope excursion corresponds to a maximum (minimum) in the long-term MS (*L**) cycle, similar to the *Elmo*.

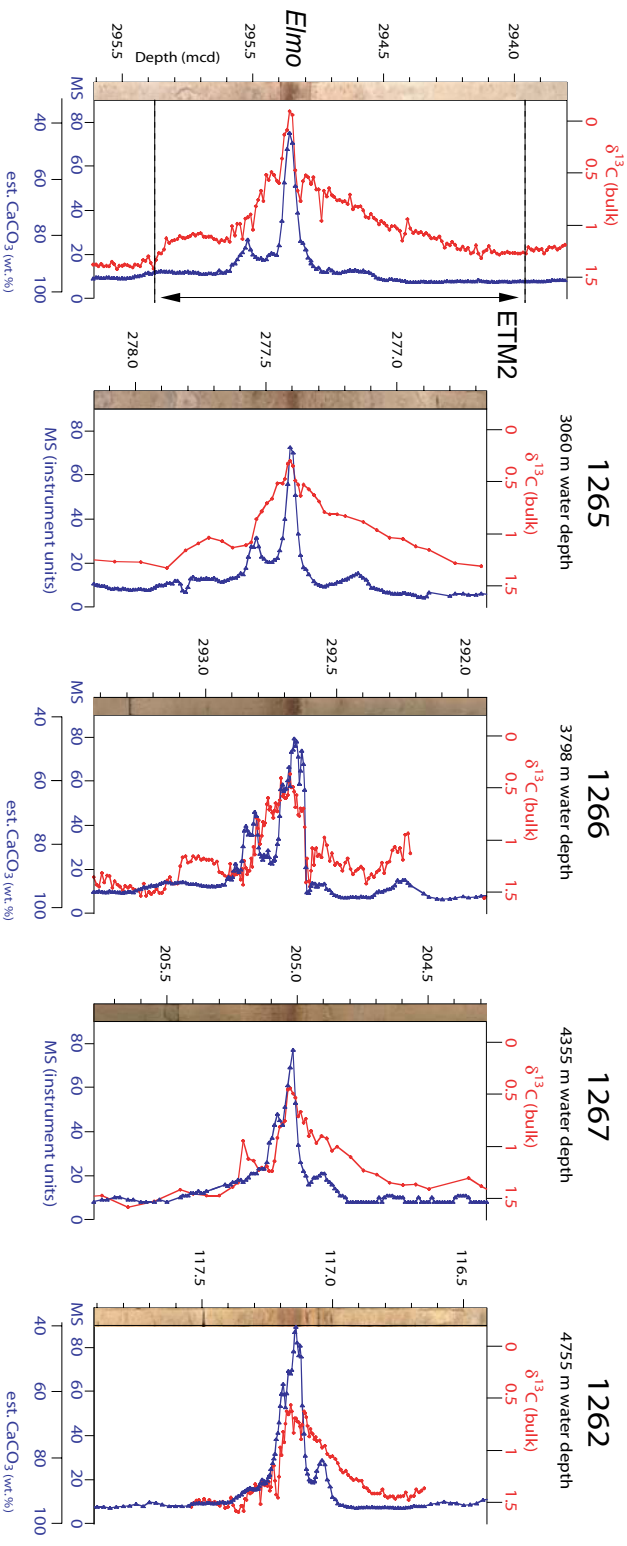

Figure 1 Bulk carbonate $\delta^{13}C$ and magnetic susceptibility (MS) records across the *Elmo* horizon at five ODP Leg 208 sites. The $CaCO_3$ wt% axes are estimates based on linear correlation with MS measurements on the same samples (Methods). Site numbers are given at the top left of each panel. Site numbers and water depths (m) are as follows: 1263, 2,717 m; 1265, 3,060 m; 1266, 3,798 m; 1267, 4,355 m; 1262, 4,755 m. Digital images of the lithology are plotted at the left site of each panel.

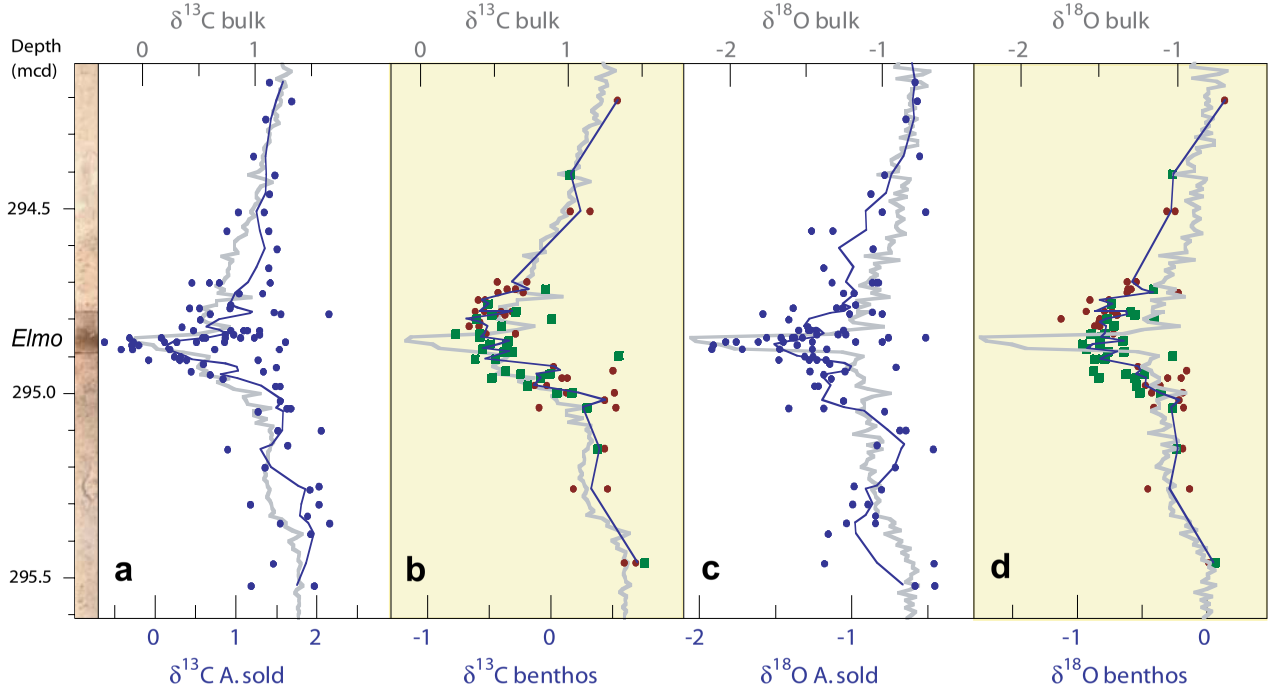

Figure 2 Stable isotope series of bulk sediment and single foraminifer specimens across the *Elmo* horizon at Site 1263. **a**, The $\delta^{13}C$ values (blue dots) of the surface dwelling planktonic foraminifer *A. soldadoensis* ($\delta^{13}C_{A.soldadoensis}$). **b**, The $\delta^{13}C$ values of the bottom dwelling benthic foraminifers ($\delta^{13}C_{benthos}$) *Cibicidoides* spp. (red squares) and *Anomalinoides* spp. (green dots). **c** and **d** as in **a** and **b** but for $\delta^{18}O$. Grey lines in **a** and **b**, and in **c** and **d**, indicate respectively the $\delta^{13}C$ and $\delta^{18}O$ values of the bulk sediment ($\delta^{13}C_{bulk}$, $\delta^{18}O_{bulk}$). Blue lines represent three-point moving averages on averaged values of duplicate analyses of a sample.

A definite tuning of the early Eocene to astronomical computations is complicated, because the precision of the orbital solution more than 45 Myr ago is limited (Varadi et al., 2003; Laskar et al., 2004). Tuning is in principle possible for the 405-kyr eccentricity cycle, because of its longer duration of stability (Varadi et al., 2003; Laskar et al., 2004) (Fig. 3). At 50 Myr ago, the absolute uncertainty in time is about 20 kyr (Laskar et al., 2004), but this did not lead to an astronomically tuned timescale owing to large uncertainties in radiometric age constraints for this time interval (Machlus et al., 2004). A second uncertainty derives from the chaotic behaviour of the inner planets related to the resonant argument $\grave{e} = (s_4\text{-}s_3) - 2(g_4\text{-}g_3)$, where g_3, g_4 are related to the precession of the perihelion and s_3, s_4 to the precession of the node of Earth and Mars (Laskar et al., 2004). This causes a large uncertainty in the determination of the time when the relatively stable ~2.4-Myr beat in eccentricity evolved from the ~1.2-Myr period when $(s_4\text{-}s_3) - (g_4\text{-}g_3) = 0$ (that is, ~2.25 Myr in the nominal La2004 (Laskar et al., 2004) and R7 (Varadi et al., 2003) solutions between 53–57 Myr ago). This problem limits an accurate age determination of successive minima in this very long eccentricity cycle and the related intervals of reduced amplitude changes in the short eccentricity cycle, and explains the offset between the ~2.25-Myr cycles of the nominal La2004 and R7 solutions in the studied time interval (Fig. 3).

Because of these uncertainties, only a floating tuning could be realized (see also Appendix 2). First, we emphasize that MS maxima (*L** minima) correlate to eccentricity maxima based on the distinct amplification of the precession-related lithological changes during the long- and short-term MS maxima (Appendix Fig. 2.4). This observation is crucial, because it implies that the carbon isotope shifts associated with the PETM and *Elmo* horizon also correspond to maxima in the long and short eccentricity cycles (Fig. 3). Second, we correlated the (on average less amplified) ~100-kyr cycles within the second (II; Fig. 3) ~405-kyr cycle to the minimum in the ~2.25-Myr cycle at 53.5 Myr ago (La2004) or 54.0 Myr ago (R7) (Appendix Fig. 2.5). Using this first order calibration, we tuned all long and short eccentricity cycles, implying that all cycles should be shifted one ~405-kyr cycle older in R7 than in the nominal La2004 solution (Fig. 3). As a result, the *Elmo* horizon correlates with the short eccentricity maximum at ~53.235 Myr ago (La2004) or ~53.620 Myr ago (R7), and the onset of the PETM carbon isotope excursion correlates with the long eccentricity maximum centred at ~55.270 Myr ago (La2004) or ~55.675 Myr ago (R7). This tuning implies that both events occurred briefly after a period of low-amplitude, short eccentricity changes associated with a minimum in the very long-term orbital perturbation of ~2.25 Myr.

The $\delta^{13}C_{bulk}$ negative shift of 1.4–1.6‰ in the Elmo horizon at Site 1263 is, with exception of the PETM carbon isotope excursion, of an unusually large

Figure 3 Astronomical tuning of the lower Eocene sediments at Walvis ridge to two different orbital computations. **a**, The extracted short (red lines) and long (grey lines) eccentricity-related cycles from magnetic susceptibility (MS) and colour reflectance (*L**) of sites 1262 and 1267 (dashed lines) represent respectively the 97.5% and 99.5% significant peaks in the CLEAN spectra (Appendix Fig. 3.4). **b**, Correlation of the long-term (I–V) and short-term (0-19) eccentricity-related maxima to their correlative cycles in the R7 (Varadi et al., 2003) (grey) and La2004 (Laskar et al., 2004) (red) orbital solutions. The 405-kyr and ~2.25-Myr cycles of eccentricity were extracted using a gaussian filter with a frequency of 0.00247±0.0001 (kyr”1) and of 0.00043±0.0001 (kyr”1), respectively.

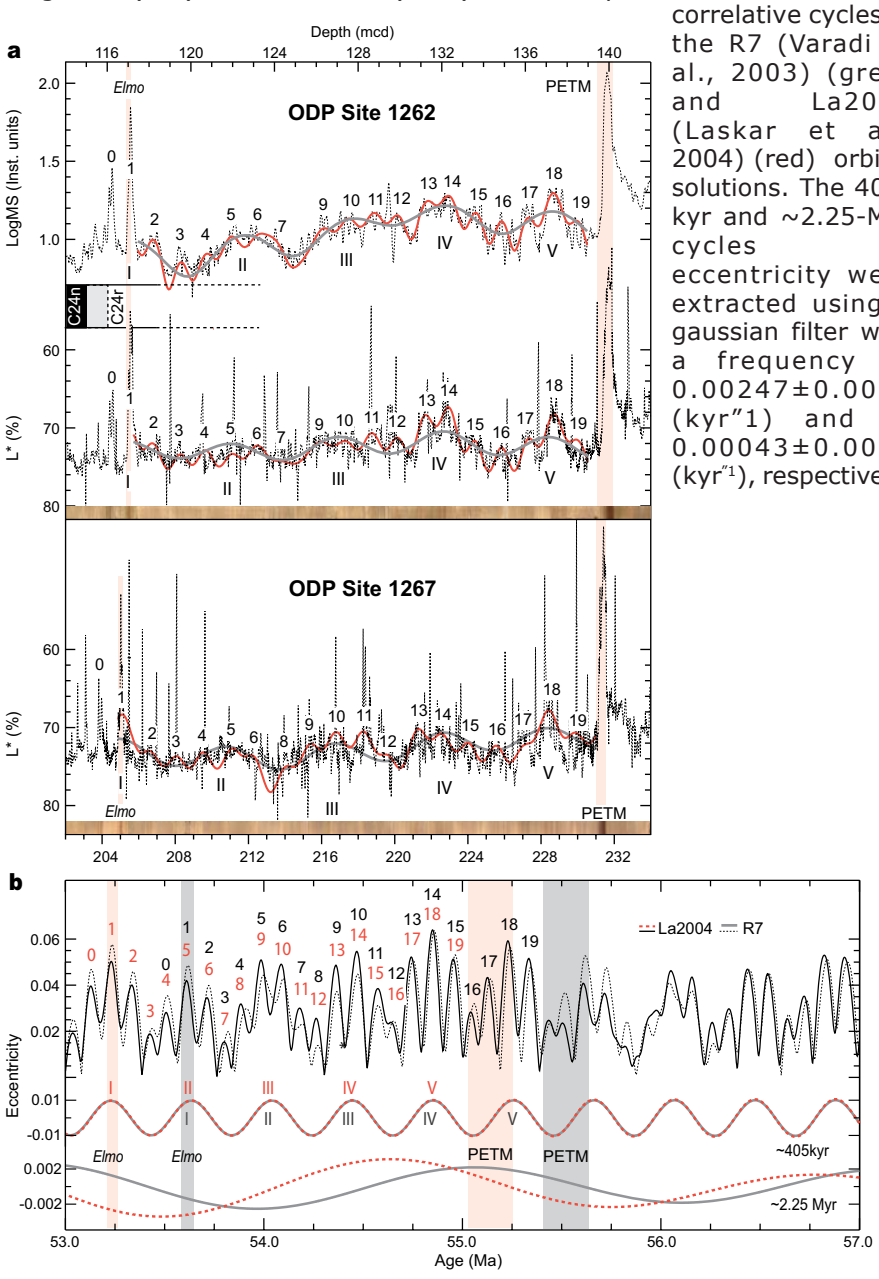

magnitude for the early Paleogene (Cramer et al., 2003). Its position just below C24n/C24r and within NP11 suggests that this excursion correlates to the ~1‰ depletion characterizing the H1 event in the North Atlantic (DSDP Site 550 and ODP Site 1051), the Southern Ocean (ODP Site 690) and the Pacific Ocean (DSDP Site 577; (Cramer et al., 2003) (see Appendix 2). Moreover, the paleosol carbonate isotope record from the Bighorn basin also shows a strong negative $\delta^{13}C$ excursion just below C24n/C24r (Koch et al., 2003), indicating that the carbon isotope excursion is global and recorded in both marine and terrestrial basins (Appendix Fig. 2.6). The Elmo horizon, however, has yet not been recognized at other locations, although the H1 event is accompanied by high MS values at Sites 550 and 690 (Cramer et al., 2003). Hence, the large drop in $CaCO_3$ wt% in the Walvis ridge cores probably indicates a major global ocean lysocline shoaling, but in contrast to the PETM (Chapter 1), the calcite compensation depth appears to have remained below the paleodepth of Site 1262. Application of the empirical temperature–$\delta^{18}O$ relationship (Shackleton, 1967; O'Neil et al., 1969) indicates furthermore that the ~1‰ $\delta^{18}O_{A.soldadoensis}$ change within the *Elmo* horizon reflects a sea surface temperature rise of at least 3 – 4°C, about half of the mid- to high-latitude sea surface temperature changes estimated for the PETM (Zachos et al., 2003). All this suggests that the Elmo horizon characterises a second pronounced early Eocene thermal maximum (ETM2; Fig. 1), similar to the PETM in both orbital and biogeochemical aspects, but of approximately half its amplitude in carbon isotope excursion, rise in sea surface temperature, and carbonate dissolution.

The linkage of both events to a similar orbital configuration disagrees with Cramer *et al.* (Cramer et al., 2003) who related the PETM to a minimum and H1 (ETM2 equivalent) to a maximum in a ~405-kyr cycle, thereby promoting the comet impact hypothesis (Kent et al., 2003). In addition, according to their tuning the interval between the PETM carbon isotope excursion and C24n/C24r should span ~1.5 Myr, which is significantly shorter than the five ~405-kyr cycles (~2 Myr) that we found. These discrepancies can probably be attributed to large uncertainties in their approach of using low-amplitude bulk carbon isotope transient excursions and counts of poorly expressed lithological cycles from incomplete successions (Cramer et al., 2003). Hence, we suggest that the extreme seasonal contrast at both hemispheres during eccentricity maxima increased intermediate seawater temperatures, thereby triggering the release of oceanic methane hydrates. In this respect, the critical conjunction of short, long and very long eccentricity cycles and the long-term late Paleocene to early Eocene warming trend may have favoured the build-up of a significant methane hydrate reservoir before its release during both events, thereby excluding unique mechanisms for explaining the PETM (Dickens et al., 1995; Thomas and Shackleton, 1996; Bralower et al., 1997; Dickens et al., 1997; Katz et al., 2001; Kent et al., 2003; Schmitz et al., 2004; Svensen et al., 2004). The less extreme signal of ETM2 may reflect the inability

of the methane hydrate reservoir to return to pre-PETM dimensions, especially under the warm conditions that prevailed in the interval spanning the two events (Zachos et al., 2001). Above ETM2 (H1) an increasing number of low-amplitude carbon transients occurred, of which the first, H2 (Cramer et al., 2003), seems to correspond with the two thin brown layers one 100-kyr cycle above the *Elmo* horizon (number 0 in Fig. 3), suggesting that the threshold for dissociation of clathrates was low during the early Eocene climatic optimum (Zachos et al., 2001), enabling even the short eccentricity cycles to trigger minor methane releases.

Methods

Sampling and $CaCO_3$ wt% analyses

Discrete sediment samples were collected at a 0.5–1-cm spacing across the *Elmo* horizon in holes 1262A, 1263C and 1266C. All samples were freeze-dried and analysed for magnetic susceptibility per gram sediment (MS g^{-1}) using an AGICO KLY-3 device. These records were compared to the split core point magnetic susceptibility (PMS) and whole core MS of the multiple sensor track (MS-MST) measurements obtained during Leg 208 (Zachos et al., 2004). We converted all MS data to the MS-MST scale by performing linear regression analyses between MS g^{-1} and PMS (Appendix Fig. 2.2) and the conversion of PMS to MS-MST using the equation MST=(PMS×2.0683)+7.8257 (R^2=0.99) (Zachos et al., 2004).

Every fourth sample (but all within the *Elmo* horizon) was used for calcium carbonate analyses. The $CaCO_3$ wt% was based on the amount of total carbon combusted with the Fison NA 1500 CNS analyser. Analytical precision and accuracy were determined by comparison with an international standard (BCR-71) and in-house standards (F-TURB, MM-91). The relative standard deviations, analytical precision and accuracy were better than 3%. Several samples prepared for palynological studies revealed that no significant amount of organic carbon was present, with an uncertainty smaller than the analytical precision. A regression analysis between the $CaCO_3$ wt% and the MS g^{-1} (converted to the MS-MST scale) was applied (Appendix Fig. 2.2) to obtain the estimated $CaCO_3$ wt% scale (Fig. 1).

Stable isotopes

Bulk stable isotope measurements were carried out for all sites with an average spacing of 4 cm, but in 0.5–1-cm resolution through the *Elmo* horizon. The isotope measurements were carried out using an ISOCARB common bath carbonate preparation device linked on-line to a VG SIRA24 mass spectrometer. Isotope values were calibrated to the PeeDee Belemnite (PDB) scale. Analytical

precision was determined by replicate analyses and by comparison to international (IAEA-CO1 and NBS19) and in-house (NAXOS) carbonate standards, showing standard deviations of <0.06‰ and <0.1‰ for $\delta^{13}C$ and $\delta^{18}O$, respectively.

Stable isotope measurements of individual planktonic and benthic foraminiferal specimens were carried out using a CARBO-KIEL automated carbonate preparation device linked on-line to a Finnigan MAT252 mass spectrometer. Specimens were hand picked from the >300 μm fraction and cleaned in ethanol in an ultrasonic bath for 30 s. Calibration to the international carbonate standard NBS19 revealed an analytical precision better than 0.03‰ and 0.05‰ for $\delta^{13}C$ and $\delta^{18}O$, respectively..